12-30-2018

Performance of C_2H_4 Reductant in Activated-Carbon-Supported MnOx-Based SCR Catalyst at Low Temperatures

Guangli Liu
PetroChina, China

Dongtai Han
China University of Mining and Technology, China

Jie Cheng
China University of Mining and Technology, China

Yongshi Feng
China University of Mining and Technology, China

Wenbin Quan
China University of Mining and Technology, China

See next page for additional authors

Authors
Guangli Liu, Dongtai Han, Jie Cheng, Yongshi Feng, Wenbin Quan, Li Yang, and Kozo Saito

Performance of C_2H_4 Reductant in Activated-Carbon-Supported MnOx-Based SCR Catalyst at Low Temperatures

Notes/Citation Information
Published in *Energies*, v. 12, issue 1, 123, p. 1-15.

Digital Object Identifier (DOI)
https://doi.org/10.3390/en12010123

energies

MDPI

Article

Performance of C_2H_4 Reductant in Activated-Carbon-Supported MnOx-based SCR Catalyst at Low Temperatures

Guangli Liu [1], Dongtai Han [2], Jie Cheng [2], Yongshi Feng [2], Wenbin Quan [2], Li Yang [2,*] and Kozo Saito [3,*]

1 Lanzhou Petrochemical Research Center, PetroChina, Lanzhou 730060, Gansu, China; liuguangli@petrochina.com.cn
2 School of Electrical and Power Engineering, China University of Mining and Technology, Xuzhou 221116, Jiangsu, China; TS17130098P2@cumt.edu.cn (D.H.); 17165520@cumt.edu.cn (J.C.); 17165501@cumt.edu.cn (Y.F.); TS16130012A3@cumt.edu.cn (W.Q.)
3 Department of Mechanical Engineering, College of Engineering, University of Kentucky, Lexington, KY 40506, USA
* Correspondence: li.yang@cumt.edu.cn (L.Y.); ksaito@uky.edu (K.S.); Tel.: +86-0516-83592000 (L.Y.); +1-859-2180639 (K.S.)

Received: 20 November 2018; Accepted: 26 December 2018; Published: 30 December 2018

Abstract: Hydrocarbons as reductants show promising results for replacing NH_3 in SCR technology. Therefore, considerable interest exists for developing low-temperature (<200 °C) and environmentally friendly HC-SCR catalysts. Hence, C_2H_4 was examined as a reductant using activated-carbon-supported MnOx-based catalyst in low-temperature SCR operation. Its sensitivity to Mn concentration and operating temperature was parametrically studied, the results of which showed that the catalyst activity followed the order of 130 °C > 150 °C > 180 °C with an optimized Mn concentration near 3.0 wt.%. However, rapid deactivation of catalytic activity also occurred when using C_2H_4 as the reductant. The mechanism of deactivation was explored and is discussed herein in which deactivation is attributed to two factors. The manganese oxide was reduced to Mn_3O_4 during reaction testing, which contained relatively low activity compared to Mn_2O_3. Also, increased crystallinity of the reduced manganese and the formation of carbon black occurred during SCR reaction testing, and these constituents on the catalyst's surface blocked pores and active sites from participating in catalytic activity.

Keywords: NOx reduction; selective catalytic reduction; manganese oxides; activated carbon; deactivation mechanism

1. Introduction

Nitric oxides (NO_X) in flue gas are a major cause of air pollution and are main contributors to photochemical smog, acid rain, and haze [1–3]. Consequently, more strict emission controls of NO_X emissions are under investigation [4]. Such NO_X control technologies like NO_X direct decomposition, selective catalytic reduction (SCR), and selective noncatalytic reduction (SNCR) have been widely examined for NO_X reduction [5,6]. Of these, the SCR of NO_X using NH_3 as a reductant (NH_3-SCR) is considered one of the most efficient approaches [7].

Catalysts play a vital role in NH_3-SCR technology; $V_2O_5/WO_3/TiO_2$ catalysts demonstrate excellent catalytic performance in stationary plants such as power plants, refineries, and so forth [8–10]. Despite its high activity, a number of obstacles still haunt this technology. Ammonia slip is a common problem because, by appropriately adjusting the amount of ammonia injected to achieve optimized

de-NO_X activity, ammonium salts (ammonium sulfate or ammonium bisulfate) will form from the ammonia slip and then deposit within downstream flow pipes in a boiler [11–13]. These deposits endanger long-term operation of the device due to fouling and blockage [7]. In addition, spent vanadium-based catalysts are considered a hazardous waste and their post-treatment is difficult and costly [14].

Furthermore, the optimal working temperature for vanadium catalysts range from 300 to 400 °C [15] with a narrow temperature operating window [7]. Hence, to meet the required temperature conditions without external heating means the catalyst has to be installed upstream of a particulate collector and desulfurization unit [16]. In contrast, if the operating temperature could be lowered to, for example, less than 250 °C, then the de-NOx step could be installed downstream of a heat recovery steam generator (HRSG). Small-scale industrial boilers like coke ovens, steel furnaces, and glass kilns operate with flue gas temperatures near 200–300 °C [8,17,18] and temperatures drop below 200 °C after a desulphurization unit. These conditions imply that currently used vanadium-based catalysts do not meet these temperature requirements [19,20]. Therefore, substantial interest has been expressed for developing low-temperature (<200 °C) SCR catalysts [21].

To date, a great number of studies have been carried out worldwide to develop low-temperature NH_3-SCR catalysts, and much progress has been made [22,23]. Based on the active component, NH_3-SCR catalysts can be divided into three categories: noble metal (Pt, Pd, Ag, etc.) catalysts, transition metal (Mn, Fe, V, Cu, Cr, Co, etc.) oxide catalysts, and transition metal (especially Cu and Fe) ion- exchanged zeolite catalysts. Noble-metal-based catalysts have been widely studied since the 1970s, and are applied mainly to engine exhaust deNO_x [24]. Though the noble metals have excellent catalytic activity at low temperature, they are costly, have a narrow operation window, and are sensitive to SO_2 [25]. Transition-metal-oxide-based catalysts are inexpensive compared to noble metal oxide catalysts, are usually more resistant to poisoning, and have substantively higher active surface areas [26–28]. As a result, transition metal oxides have become technically and economically effective catalysts for SCR of NOx at low temperatures with MnOx, FeOx, and CuOx drawing the most attention [26]. Mn-based catalysts have displayed high NO_X conversion during NH_3-SCR de-NO_X over a wide reaction temperature range (160–400 °C) [29].

For example, Mn/beta have been determined to have NO_X conversion levels near 97.5% at 240 °C while maintaining >90% conversion within a temperature range of 220–350°C [30]. Iron-based catalysts also have demonstrated high activity and low toxicity compared to the V_2O_5-WO_3 (MoO_3)/TiO_2 catalysts [17,31]. Pure Fe_2O_3 [7] has exhibited well-defined activity with nearly 95% conversion with an operation temperature window of 250–400 °C; Cu-based catalysts may have an advantage of applicability because of good low-temperature activity and low cost, but to date, its NO_X conversion rates have been relatively low [32–34]. In comparison, MnOx-based catalysts have had higher NO_x conversion when using low reaction temperatures [35,36].

Although NH_3 is almost universally used as the reductant in SCR de-NO_X reactions [1,7,18], it is dangerous with significant safety issues associated with usage, transportation, and storage [37,38]. In contrast, C_2H_4 as a reductant for de-NOx reactions (i.e. HC-SCR) under lean conditions is more easily implemented and has fewer safety issues [39–41]. The overall reaction equation of HC-SCR can be written as:

$$C_xH_y + 2\ NO + (x + 0.25y - 1)\ O_2 = N_2 + x\ CO_2 + 0.5y\ H_2O$$

There is rich literature reporting the development of catalysts for HC-SCR and other usages [42]. Using hydrocarbon reductants, noble metals have shown high catalytic activity at low temperatures [43,44]. For example, Pt/Zr-SiO_2 gave high NO conversion at temperatures of 50–300 °C using CO + H_2 as the reductant [45]. However, the cost of noble-metal-based catalysts is very high and thus not favorable for large-scale applications, whereas transition metal oxides are significantly less expensive and demonstrate high activity at low temperatures and are environmentally friendly to dispose of or recycle after their use; as a consequence, these metal oxides have become a main focus in HC-SCR catalyst development [25,46].

For example, Komvokis et al. studied the C_3H_6-SCR deNOx activity of Cu-exchanged ZSM-5 samples under dry reaction conditions and found that the catalytic activity was significantly enhanced by increasing the Cu loading from 0.5 to 1.5 wt.% [47]. This study also showed that the active temperature window could be lowered to almost 100 °C by adding promoters. Other transition metal oxides like MnO_X also have demonstrated excellent $deNO_X$ performance at low temperatures [48]. However, deactivation of transitional metal oxides can be significant when real feeds are used that contain the presence of water and/or SO_2 [48]. To diminish deactivation, the doping of other metals has demonstrated higher, sustained activity for transition-metal-based catalysts [49]. For example, noble metal or Sn doping has been shown to be effective against deactivation [50].

The supports used for the active SCR catalytic materials have included inert metal oxides like Al_2O_3, TiO_2, SiO_2, and activated carbon (AC); the oxides exhibit high temperature stability and excellent mechanical properties [15] while AC has demonstrated high chemical stability and surface area with low cost [45,51–54].

Using AC as an SCR catalyst support with NH_3 as a reductant has been examined [55]; Tang et al. [53] showed that over 90% NO_X conversion was possible with manganese/AC catalysts during NH_3-SCR reaction testing with a temperature range of 150–250 °C. Although ammonia slip occurred, the ammonium sulfate salts that were formed were also more easily reduced because, perhaps, of the AC promoting reduction of the salts, thereby avoiding their extensive accumulation on catalyst surfaces [56].

However, few studies have examined AC-supported transition metal oxides during HC-SCR reactions [7]. Because MnOx has exhibited promising low-temperature HC-SCR reactivity and AC supports have excellent stability and low rates of ammonium salts accumulation [25,50,57,58], this study aimed to investigate the low-temperature catalytic performance of manganese/AC catalysts while using C_2H_4 as a reductant. Besides the reaction testing, deactivation mechanisms were also examined using SEM/EDS, X-ray diffraction (XRD), Raman spectroscopy, transmission electron microscope and selected area electron diffraction (TEM-SAED), and X-ray photoelectron spectrometer (XPS). The physical and chemical characterization provided insights for future catalyst developments and modification to eliminate or mitigate undue deactivation.

2. Experimental Methods

2.1. Catalyst Preparation

The AC used is commercially available and had a particle size of 1000–2350 μm. The raw AC was pretreated at room temperature in 10% HNO_3 for 4 h, washed until the pH of the wash solution became neutral, and then the AC was dried in air at 140 °C for 14 h. These HNO_3-treated AC supports are denoted as NAC in the following.

The precursor of the MnOx was Mn $(NO_3)_2 \cdot 4H_2O$ in water. The NAC supports were impregnated with these solutions to achieve approximate Mn loadings of 3.0 wt.%, 5.0 wt.%, and 7.0 wt.% during which time the mixtures were sonicated in a bath for 2 h. After the mixtures were allowed to stand for 12 h, they were dried at 110 °C in a vacuum oven and then calcined at 400 °C for 2 h in a sealed muffle furnace under N_2 atmosphere. The synthesized materials were labeled as Mn(0.0X)/NAC, where (X = 3, 5, 7).

2.2. Catalyst Characterization

The synthesized materials were characterized for their physical and chemical properties before and after reaction testing. Surface area and porosity were measured in a Micromeritics ASAP 2020 analyzer after degassing overnight at 160 °C and then subjected to isothermal N_2 adsorption–desorption measurements at 77 K. Crystalline structures were examined by X-ray diffraction (XRD) using CuKα irradiation in a Rigaku SmartLab system with a 2θ range of 2–75°. The microstructure was observed by scanning electron microscopy (SEM) performed on an FEI Quanta 250 embedded with a Bruker

Quantax EDS. Raman spectroscopy (Horiba Jobin Yvon LabRam HR) was used to investigate the molecular speciation of the catalyst when irradiated by a 442 nm laser frequency that minimized sample fluorescence. The laser was focused on the samples with a confocal microscope using a 50 X objective (Olympus BX-30-LWD, NA = 0.5); the spectral resolution was 2 cm^{-1}, and wavenumber calibration was checked using the silica vibrational mode at 520.7 cm^{-1}. TEM-SAED was performed on Tecnai G2 F20 instrument (FEI Co., USA). Catalyst was ultrasonicated in ethanol for 15 min, the solvent was filtered, and samples were obtained on carbon-supporting film for the test. XPS was performed on Thermo Fisher ESCALAB 250Xi instrument, with Al Kα excitation, and the data was calibrated using the C1s peak at 284.8 eV.

2.3. Catalytic Activity Test

The experiment setup for testing catalytic activity is shown in Figure 1. It included a fixed-bed, quartz tube reactor (i.d. = 20 mm) heated by a temperature-controlled furnace; during testing, the weight of the sample was 10 g. Gas flow rates were controlled at 1500 ml/min by a set of mass flow controllers (MFCs, MF SHY 400) which produced a simulated gas mixture of 500 ppm NO, 500 ppm C_2H_4, 3 vol.% O_2, and N_2 as a balance. The gas mixture was flowed into the reactor after the temperature attained a stable state and gas concentrations of outlet NO and NO_X were analyzed using a flue gas analyzer (MRU). NO conversion and NO_2 selectivity were evaluated according to the following equation:

$$\text{NO conversion } (\%) = \left(1 - \frac{[NO]_{out}}{[NO]_{in}}\right) \times 100 \quad (1)$$

$$NO_2 \text{ selectivity } (\%) = \frac{[NO_2]_{out}}{[NO]_{in}} \times 100 \quad (2)$$

where the subscripts in and out indicate the inlet and outlet concentrations, respectively.

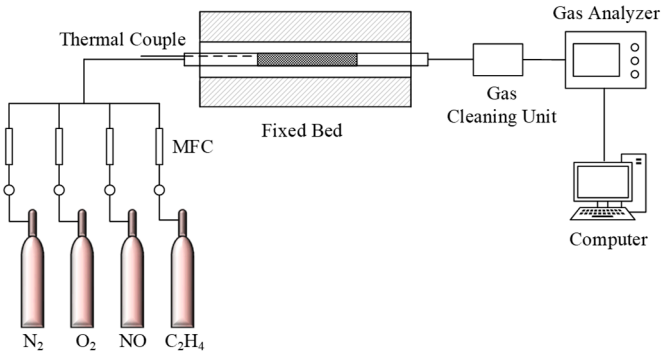

Figure 1. Schematic diagram of the bench-scale setup.

3. Results and Discussion

3.1. Dispersion of Active Component

The morphologies of the NAC and Mn(0.03)/NAC were examined before testing using SEM/EDS data which are presented in Figure 2. The NAC had a porous surface structure, as was also confirmed by its 710 m^2/g BET surface area. The morphology of Mn (0.03)/NAC showed a morphology similar to the AC by itself, suggesting that the Mn species was well dispersed on the AC surface without significant agglomeration.

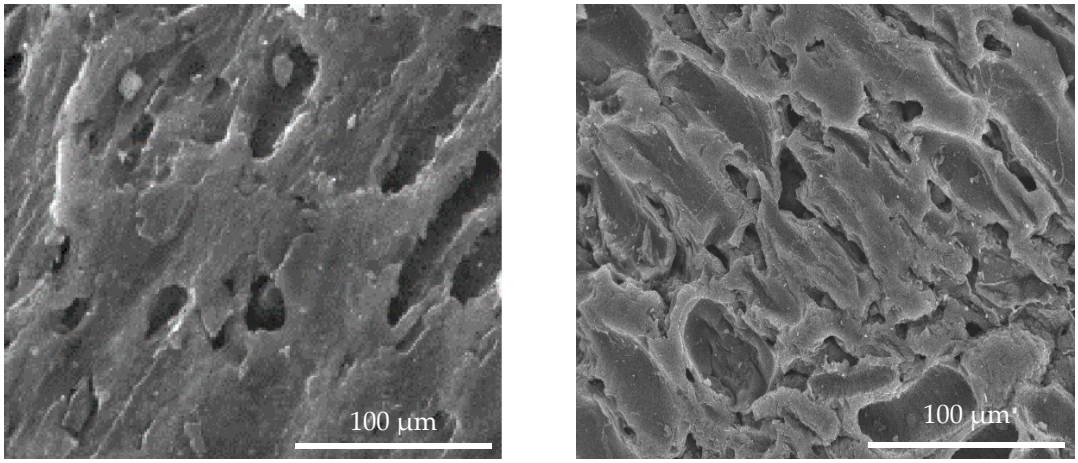

(**a**) (**b**)

Figure 2. SEM images of (**a**) HNO_3-treated Activate Carbon (NAC); (**b**) Mn (0.03)/NAC.

EDS data from Mn(0.03)/NAC are shown in Figure 3; the elements detected were C, O, Mn, Si, and Al with C and O the main constituents. The relatively small amounts of Si and Al were expected to originate from ash of the original precursor to the AC before it was processed into activated carbon. For this sample, the Mn concentration was 2.82 wt.%, a value close to the theoretical value of 3.0 %. The EDS mapping of Mn species in Figure 4 further demonstrated that Mn was highly distributed on the surface and contained insignificant Mn agglomerates.

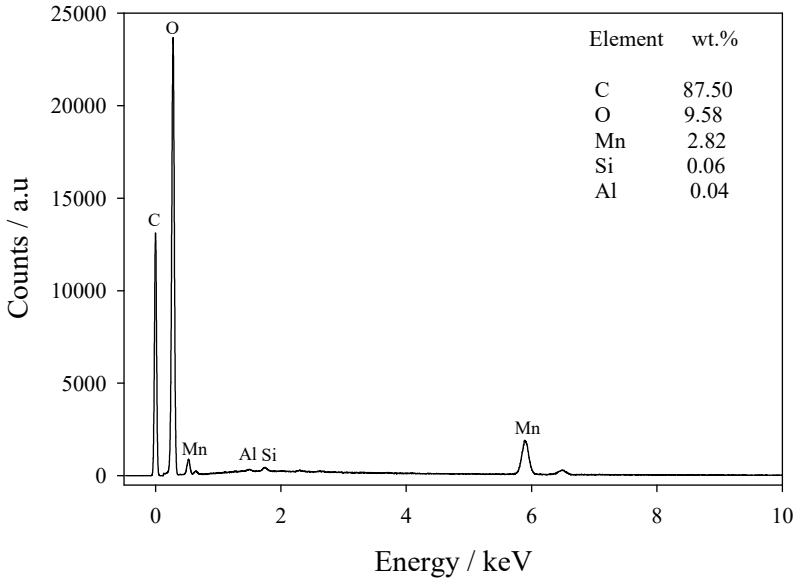

Figure 3. EDS data and elemental mass fractions for Mn (0.03)/NAC.

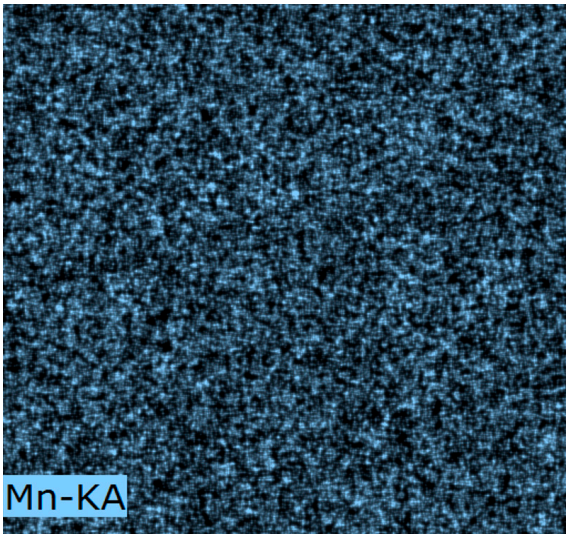

Figure 4. Dispersion of Mn Element in Mn (0.03)/NAC by EDS mapping.

3.2. Catalytic Performance

As can be seen in Figure 5, all three catalysts produced excellent NO conversion of close to 100% in the first 30 minutes of reaction time at all of the temperatures tested, indicating that they may be effective for low-temperature HC-DeNOx applications. However, they experienced rapid decreases in conversion with decrease rates having an order of 130 °C < 150 °C < 180 °C; after 2 h of reaction testing, the NO conversions for all three test conditions were less than 30%, indicating the overall integrated activity was poor. N_2O using gasbag sampling was measured by GC to less than 2 ppm—considered too minor for discussion, therefore, not discussed in this study. The initial NO_2 selectivity was very low and near 0% during the first 20 min of testing, as shown in Figure 5b. For reaction temperatures of 130 °C and 150 °C, the NO_2 selectivity remained at less than 10% during the entire tests.

Similar to the data in Figure 5, the NO conversion and NO_2 selectivity in Figure 6 for the catalysts with three different Mn loadings had high initial conversion activity and very low NO_2 selectivity which then the NO conversion began to decrease and the NO_2 selectivity began to increase ~30 min after the testing was begun; NO conversion for these loadings followed the order 3% < 5% < 7% and NO_2 selectivity had an order of 7% ~ 5% < 3%. During deactivation, the NO conversion dropped to between 20 and 35% whereas the NO_2 selectivity increased to 10–25%.

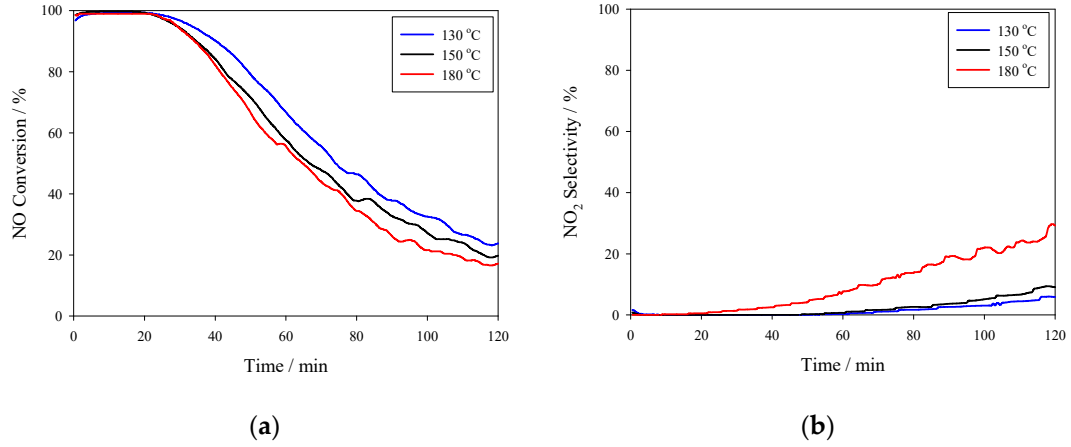

(**a**) (**b**)

Figure 5. Catalytic performance of Mn (0.03)/NAC using C_2H_4 as a reductant. The reaction temperature varied from 130 to 180 °C; reaction conditions were 500 ppm NO, 500 ppm C_2H_4, and 3% O_2 at a flow rate of 1500 mL/min. (**a**) NO conversion; (**b**) NO_2 selectivity.

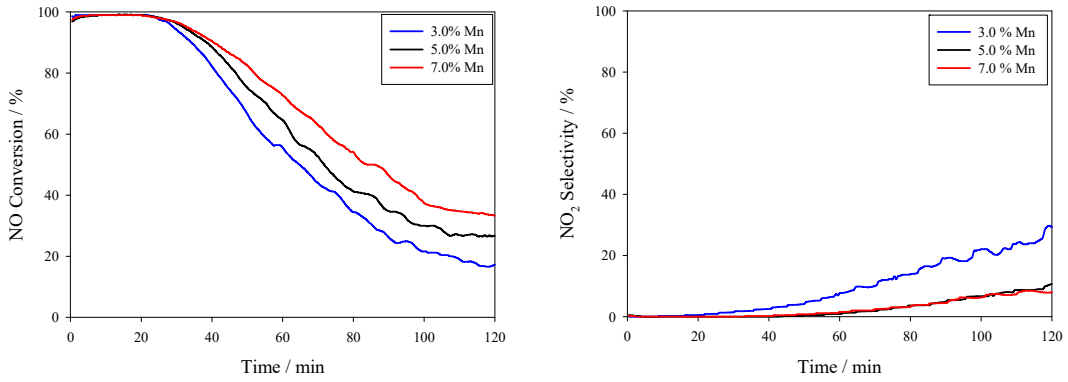

(**a**) (**b**)

Figure 6. NO Conversion of Mn (0.0X)/NAC (X = 3, 5, 7) using C_2H_4 as a reductant. The reaction temperature was 180 °C and the reaction conditions were 500 ppm NO, 500 ppm C_2H_4, and 3% O_2 at a flow rate of 1500 mL/min. (**a**) NO conversion; (**b**) NO_2 selectivity.

Although the NO conversion of these Mn (0.0X)/NAC catalysts exhibited rapid decreases with only 2 h of testing, their initial reactivity at 130 °C was superior than most other HC-SCR catalysts, including vanadium, iron-based zeolites, and noble metal oxide catalysts [56]. Hence, insight into their reactivity and its decline may be worthwhile to explore and, for this reason, the mechanisms of deactivation were assessed using a variety of physical and chemical probes.

3.3. Deactivation Mechanism

3.3.1. Surface Area and Porosity

Changes in surface areas and porosities were assessed because it is well accepted that micropores and mesopores are a key for catalytic activity in which micropores favor dispersion of the active component and mesopores guarantee accessibility of the reactants to the interior of the micropores within a catalyst [59,60]. Table 1 shows that the BET surface area, average pore size, and pore volume of the Mn (0.03)/NAC catalyst did not change significantly from before to after reaction testing; their decreases after 2 h of testing were only 4–8% whereas the NO conversion had decreased by 80%. These comparisons suggest that surface area and porosity decreases were likely not the cause of decreased activity.

Table 1. Surface area and porosity.

	BET Surface Area (m^2/g)	Average Pore Width (nm)	Pore Volume (cm^3/g)
Mn(0.03)/NAC Before Reaction	668.54	2.46	0.41
Mn(0.03)/NAC After Reaction	632.62	2.37	0.375

3.3.2. Morphology Evolution

The morphology of Mn (0.03)/NAC catalyst was examined using SEM after HC-SCR reaction testing, as displayed in Figure 7, and these results were compared to the SEM data displayed in Figure 2. In general, the surface of the used catalyst contained considerable numbers of aggregates which were not present before testing. These aggregates were porous and shapeless, and had varied sizes; their presence, however, did not significantly decrease the surface area and porosity of the catalyst. It is possible that these aggregates provided additional surfaces to supplement other surface area and porosity losses within the original catalyst structure during deactivation. These aggregates could also represent agglomeration sites of the originally active catalytic components, and thereby greatly affect active site dispersion to cause rapid deactivation.

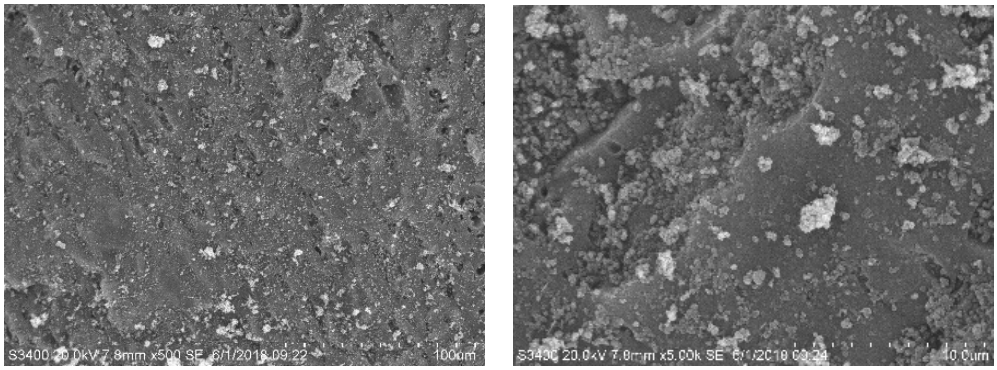

(**a**) (**b**)

Figure 7. Morphology of Mn (0.03)/NAC after reaction testing. (**a**) SEM image Mn (0.03)/NAC, 500 X; (**b**) SEM image Mn (0.03)/NAC, 5000 X.

3.3.3. Crystalline Phase Change

Well-dispersed catalytic components usually have low crystallinity or high disorder that broadens their XRD peaks to the point of nondetection, whereas poorly dispersed or aggregated catalytic components usually have narrower XRD peaks that are easily detected. A comparison of the XRD patterns of the fresh and used Mn (0.03)/NAC catalyst before and after reaction testing is shown in Figure 8; both have a broad, medium-intensity peak at 2θ = 24° and a weak peak at 2θ = 43° which correlate with characteristic XRD peaks of amorphous carbon structures [59]. The catalyst before reaction did not have any other XRD peaks; this fact suggests highly dispersed, noncrystalline Mn, whereas after reaction testing, two narrow, medium-intensity peaks were established with one at 2θ = 26°and the other at 2θ = 50°. These peaks are characteristic of crystalline Mn_3O_4. Hence, the Mn oxide species in the fresh catalyst did agglomerate into larger crystalline Mn_3O_4 species during testing. Besides decreased dispersion causing activity losses, it is also known that SCR catalytic activity of Mn_3O_4 species is relatively low, following the order of MnO_2 > Mn_2O_3 > Mn_3O_4 > MnO. Hence, both decreased Mn dispersion and the formation of low-activity Mn_3O_4 are responsible, in part, for rapid decreases in catalytic activity with time of reaction testing.

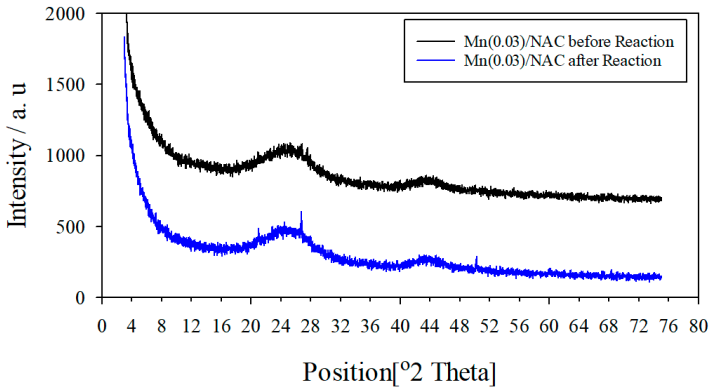

Figure 8. XRD pattern of Mn (0.03)/NAC catalyst before and after reaction testing.

3.3.4. Raman Spectra

Figure 9 displays the Raman spectra of the Mn (0.03)/NAC catalyst before and after reaction testing. Both spectra have a peak at 1357 cm^{-1} (D) and 1643 cm^{-1} (G), and bands in the 2700–3100 cm^{-1} region (2D); the characteristics and locations of these point to Raman scattering from the AC itself [61]. Although a very weak band is apparent at 643 cm^{-1} in the fresh catalyst, its intensity is enhanced greatly in the used catalyst. Reference spectra of Mn_3O_4 show an intense peak at 650 cm^{-1} (A_{1g})

corresponding to the symmetric stretching of the Mn–O bonds, and weaker bands at 480 (T_{2g}), 370 (E_g), 325 (T_{2g}), and 295 (T_{2g}) cm^{-1} [62]. In comparison, the Raman spectra of the Mn (0.03)/NAC catalyst after reaction testing have peaks at 647, 479, and 365 cm^{-1}, positions of which are consistent with the presence of Mn_3O_4 and in agreement with the speciation reported in other studies [63]. Therefore, Mn_3O_4 is present in the deactivated catalyst whereas before testing, the manganese oxide was more disordered then after testing; the Raman results are consistent with the XRD data.

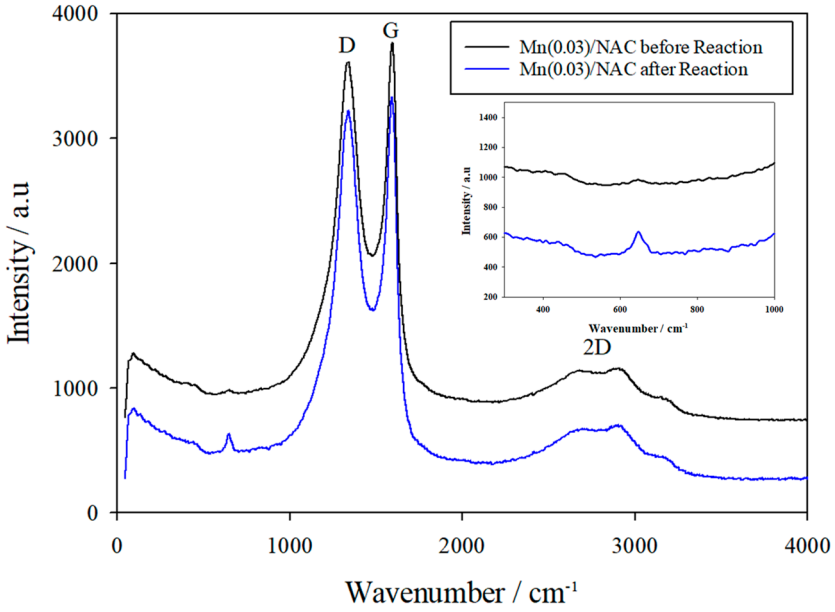

Figure 9. Raman Spectra of Mn (0.03)/NAC catalyst before and after reaction testing.

3.3.5. TEM-SAED and XPS

To further identify the formation of Mn_3O_4, TEM-SAED and XPS test of the Mn (0.03)/NAC after reaction were performed. Figure 10 shows the TEM-SAED result; the image gave bright diffraction rings, which are in agreement with the (101), (112), (103), (202), (220), and (105) planes of Hausmannite Mn_3O_4 phase, and also (002) plane of graphene was recognized. The XPS survey and high-resolution spectra of Mn 2p are shown in Figure 11; the survey scan analysis was carried out in the binding energy between 0–1350 eV, and its spectrum showed the strong peaks of Mn, C, and O, and weak peaks of Si and N were also detected due to the small amount of impurities that naturally exist in activated carbon. In Figure 11b, the high-resolution Mn 2p spectra consisted of Mn $2p_{1/2}$ and Mn $2p_{3/2}$ peaks, and the binding energy of Mn $2p_{3/2}$ was 641.2 eV, and the energy separation between the Mn $2p_{3/2}$ and Mn $2p_{1/2}$ was 11.6 eV, which well matched the values of Hausmannite Mn_3O_4 [64,65]. Those results clearly confirmed the appearance of Mn_3O_4 in the deactivated catalyst.

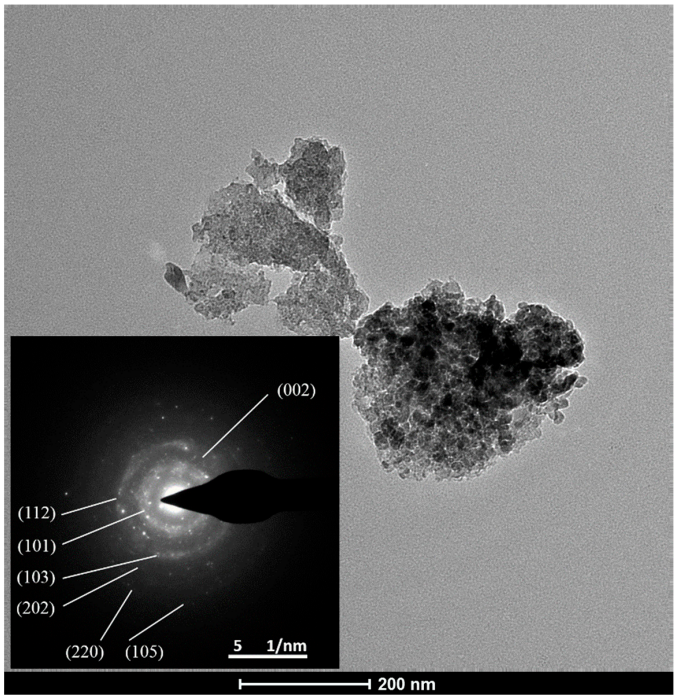

Figure 10. TEM-SAED result of Mn (0.03)/NAC after reaction.

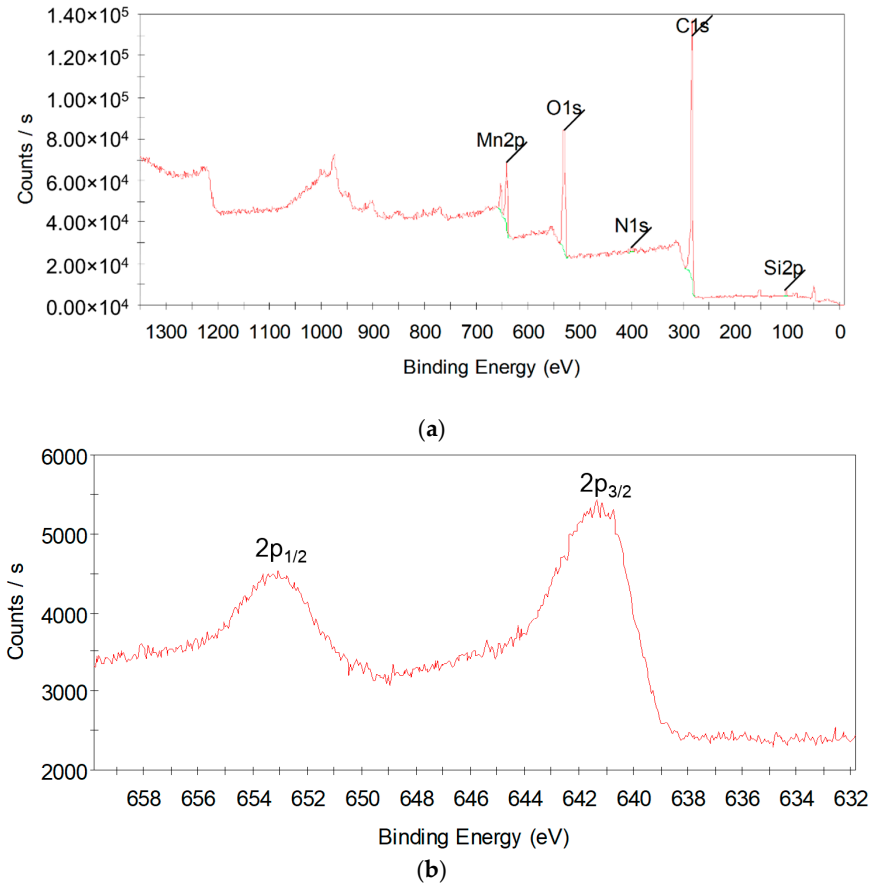

Figure 11. XPS spectra of Mn (0.03)/NAC after reaction: (**a**) survey; (**b**) high resolution of Mn 2p.

3.3.6. Formation of Carbon Spheres

Besides Mn-containing agglomerates on the surface of the carbon, some pores of the activated carbon in tested catalysts contained spheres, as shown in Figure 12. The elemental composition of these spheres is listed in Table 2; according to SEM/EDS data, they contained 90.0 wt.% carbon and 1.4% Mn. Because the monitoring diameter and depth of EDS was approximately 10 μm, it is possible that Mn within the pores of the catalyst separate from the spheres themselves was also detected. These spheres were most prevalent in part of the tested catalyst, meaning that their formation was associated with catalytic activity. It is known that MnOx decomposes hydrocarbons at low temperatures near 200 °C and forms carbon black [15]. Hence, the spheres are expected to be a type of carbon black that is deposited within the pores during the decomposition of C_2H_4. These carbon spheres may cover the manganese oxides [43] and cause some blockage of the pores, and thereby also diminish the HC-SCR activity.

In brief, the deactivation of catalysts might have two reasons. First, the manganese oxides on the supports, acting as active sites of the catalyst, were reduced to Mn_3O_4 during reaction testing and decreased the catalytic activity, since manganese oxide reactivity is known to have the following decreasing order: $MnO_2 > Mn_2O_3 > Mn_3O_4 > MnO$ [29,55]. In addition, increased crystallinity of the manganese oxides and deposition of carbon black on the catalyst's surface during SCR reaction testing caused blockage of pores and encapsulation of active MnOx sites on the NAC surface.

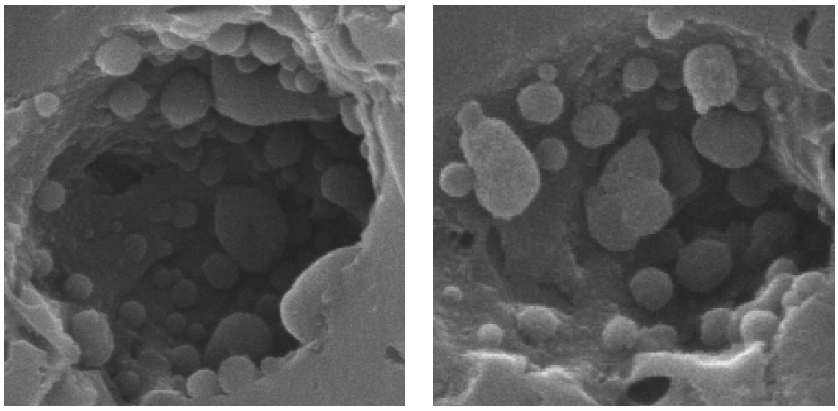

(**a**) (**b**)

Figure 12. SEM images of carbon balls: (**a**) carbon balls-1; 10000 X; (**b**) carbon balls-2; 10000 X.

Table 2. Element concentration.

Element	wt.%	at.%	Error (3 Sigma)
Carbon	89.97	92.98	35.26
Oxygen	8.65	6.71	7.75
Manganese	1.37	0.31	0.27

4. Conclusions

A series of Mn (0.0X)/NAC catalysts was prepared by impregnation, tested for catalytic activity during the reduction of NO using C_2H_4 as a reductant, and then characterized to develop information regarding trends in NO conversion. These studies have led to the following conclusions:

(1) The HNO_3-treated activated carbon contained a high surface area and significant pore volume to act as a support for the impregnation of manganese oxide; changes in the surface areas and pore volumes as a consequence of catalytic testing were insignificant.

(2) Three manganese concentrations were impregnated onto the NAC (3%, 5%, and 7%) to create Mn (0.0X)/NAC catalysts that initially exhibited nearly 100% NO conversion at temperatures

between 130 and 180 °C for up to 30 min after beginning NO conversion testing. Independent of the temperature and the manganese concentration, the conversion activity decreased rapidly beyond 30 min of testing and attained only ~20–30% conversion after 2 h.

(3) According to XRD, Raman, SEM-EDS, TEM-SAED, and XPS data, the as-prepared catalysts contained highly dispersed and highly disordered manganese species, whereas after testing, the catalysts contained crystalline Mn_3O_4 species.

(4) The deactivation of the low-temperature HC-SCR catalyst is attributed to two causes: (a) although the manganese oxide on the NAC support was initially highly active for de-NOx conversion, it was reduced to Mn_3O_4 during reaction testing, a species having less activity than MnO_2 and Mn_2O_3; (b) simultaneously, the crystallinity of the manganese oxides and their size were increased during reaction testing, and carbon black was formed that contained encapsulated manganese; the carbon black in the shape of spheres were deposited within pores and covered the active manganese sites on the NAC surface.

The above conclusions point to additional testing in which improvement in the stability of the highly dispersed Mn/AC catalysts would be sought.

Author Contributions: Conceptualization, L.Y.; Methodology, D.H.; Formal Analysis, L.Y.; Investigation, J.C., Y.F., and W.Q.; Writing-Original Draft Preparation, D.H. and L.Y.; Writing-Review & Editing, G.L., L.Y., and K.S.

Funding: This research was funded by the Natural Science Foundation of Jiangsu Province with grant number BK20180645.

Acknowledgments: The author thanks John Stencel for his valuable comments.

Conflicts of Interest: The authors declare no conflict of interest.

References

1. Kumar, P.A.; Jeong, Y.E.; Ha, H.P. Low temperature NH_3-SCR activity enhancement of antimony promoted vanadia-ceria catalyst. *Catal. Today* **2017**, *293–294*, 61–72. [CrossRef]
2. Pourkhalil, M.; Izadi, N.; Rashidi, A.; Mahboobeh, M. Synthesis of CeOx/γ-Al_2O_3 catalyst for the NH_3-SCR of NOx. *Mater. Res. Bull.* **2018**, *97*, 1–5. [CrossRef]
3. Nam, K.B.; Kwon, D.W.; Hong, S.C. DRIFT study on promotion effects of tungsten-modified Mn/Ce/Ti catalysts for the SCR reaction at low-temperature. *Appl. Catal. A-Gen.* **2017**, *542*, 55–62. [CrossRef]
4. Ying, W.; Fan, H.; Wang, R. Transition metals (Co, Zr, Ti) modified iron-samarium oxide as efficient catalysts for selective catalytic reduction of NOx at low-temperature. *Appl. Surf. Sci.* **2018**, *459*, 63–73.
5. Prieto-Centurion, D.; Eaton, T.R.; Roberts, C.A.; Fanson, P.T.; Notestein, J.M. Catalytic reduction of NO with H_2 over redox-cycling Fe on CeO_2. *Appl. Catal. B-Environ.* **2015**, *168–169*, 68–76.
6. Chakraborty, S.; Nayak, S.C.; Deo, G. TiO_2/SiO_2 supported vanadia catalysts for the ODH of propane. *Catal. Today* **2015**, *254*, 62–71. [CrossRef]
7. Muzio, L.; Bogseth, S.; Himes, R.; Chien, Y.C.; Dunn-Rankin, D. Ammonium bisulfate formation and reduced load SCR operation. *Fuel* **2017**, *206*, 180–189. [CrossRef]
8. Yu, J.; Li, C.M.; Guo, F.; Gao, S.Q.; Zhang, Z.G.; Matsuoka, K.; Xu, G.W. The pilot demonstration of a honeycomb catalyst for the DeNOx of low-temperature flue gas from an industrial coking plant. *Fuel* **2018**, *219*, 37–49. [CrossRef]
9. Luo, S.; Zhou, W.; Xie, A.; Wu, F.; Yao, C.; Li, X.; Liu, T. Effect of MnO_2 polymorphs structure on the selective catalytic reduction of NOx with NH_3 over TiO_2–Palygorskite. *Chem. Eng. J.* **2016**, *286*, 291–299. [CrossRef]
10. Yang, J.; Ma, H.; Yamamoto, Y.; Yu, J.; Xu, G.; Zhang, Z.; Suzuki, Y. SCR catalyst coated on low-cost monolith support for flue gas denitration of industrial furnaces. *Chem. Eng. J.* **2013**, *230*, 513–521. [CrossRef]
11. Colombo, M.; Nova, I.; Tronconi, E. A simplified approach to modeling of dual-layer ammonia slip catalysts. *Chem. Eng. Sci.* **2012**, *75*, 75–83. [CrossRef]
12. Li, C.; Shen, M.; Wang, J.; Wang, J.; Zhai, Y. New insights into the promotional mechanism of ceria for activity and ammonium bisulfate resistance over V/WTi catalyst for selective catalytic reduction of NO with NH_3. *Appl. Catal. A-Gen.* **2018**, *560*, 153–164. [CrossRef]

13. Chegrouche, S.; Kebir, A. Study of ammonium uranyl carbonate re-extraction-crystallization process by ammonium carbonate. *Hydrometallurgy* **1992**, *28*, 135–147. [CrossRef]
14. Gummow, B. *Vanadium: Environmental Pollution and Health Effects*; Elsevier Press: Burlington, NJ, USA, 2011; pp. 628–636.
15. Liu, C.; Shi, J.W.; Gao, C.; Niu, C. Manganese oxide-based catalysts for low-temperature selective catalytic reduction of NOx with NH_3: A review. *Appl. Catal. A-Gen.* **2016**, *522*, 54–69. [CrossRef]
16. Heck, R.M. Catalytic abatement of nitrogen oxides–stationary applications. *Catal. Today* **1999**, *53*, 519–523. [CrossRef]
17. Männikkö, M.; Skoglundh, M.; Ingelsten, H.H. Selective catalytic reduction of NOx with methanol over supported silver catalysts. *Appl. Catal. B-Environ.* **2012**, *119–120*, 256–266. [CrossRef]
18. Thirupathi, B.; Smirniotis, P.G. Co-doping a metal (Cr, Fe, Co, Ni, Cu, Zn, Ce, and Zr) on Mn/TiO_2 catalyst and its effect on the selective reduction of NO with NH_3 at low-temperatures. *Appl. Catal. B-Environ.* **2011**, *110*, 195–206. [CrossRef]
19. Chen, C.; Cao, Y.; Liu, S.; Chen, J.; Jia, W. Review on the latest developments in modified vanadium-titanium-based SCR catalysts. *Chin. J. Catal.* **2018**, *39*, 1347–1365. [CrossRef]
20. Chen, Z.H.; Li, X.H.; Yang, Q.; Li, H.; Gao, X.; Jiang, Y.B.; Wang, F.R.; Wang, L.F. Removal of nox using novel fe-mn mixed-oxide catalysts at low temperature. *Acta Phys.-Chim. Sin.* **2009**, *25*, 601–605.
21. Huang, B.; Huang, R.; Jin, D.; Ye, D. Low temperature SCR of NO with NH_3 over carbon nanotubes supported vanadium oxides. *Catal. Today* **2007**, *126*, 279–283. [CrossRef]
22. Shan, W.; Song, H. Catalysts for the selective catalytic reduction of NOx with NH_3 at low temperature. *Catal. Sci. Technol.* **2015**, *5*, 4280–4288. [CrossRef]
23. Zhang, S.; Zhang, B.; Liu, B. A review of Mn-containing oxide catalysts for low temperature selective catalytic reduction of NOx with NH_3: Reaction mechanism and catalyst deactivation. *RSC Adv.* **2017**, *7*, 26226–26242. [CrossRef]
24. Isabella, N.; Enrico, T. *Urea-SCR Technology for deNOx after Treatment of Diesel Exhausts*; Springer Press: New York, NY, USA, 2014.
25. Boningari, T.; Smirniotis, P.G. Impact of nitrogen oxides on the environment and human health: Mn-based materials for the NOx abatement. *Curr. Opin. Chem. Eng.* **2016**, *13*, 133–141. [CrossRef]
26. Yu, J.; Guo, F.; Wang, Y.; Zhu, J.; Liu, Y.; Su, F.; Gao, S.; Xu, G. Sulfur poisoning resistant mesoporous Mn-base catalyst for low-temperature SCR of NO with NH_3. *Appl. Catal. B-Environ.* **2010**, *95*, 160–168. [CrossRef]
27. Saqer, S.; Kondarides, D.; Verykios, X. Catalytic oxidation of toluene over binary mixtures of copper, manganese and cerium oxides supported on g-Al_2O_3. *Appl. Catal. B-Environ.* **2011**, *103*, 275–286. [CrossRef]
28. Lahousse, C.; Bernier, A.; Grange, P.; Delmon, B.; Papaefthimiou, P.; Ioannides, T.; Verykios, X. Evaluation of g-MnO_2 as a VOC removal catalyst: Comparison with a noble metal catalyst. *J. Catal.* **1998**, *178*, 214–225. [CrossRef]
29. Sultana, A.; Sasaki, M.; Hamada, H. Influence of support on the activity of Mn supported catalysts for SCR of NO with ammonia. *Catal. Today* **2012**, *185*, 284–289. [CrossRef]
30. Xu, W.; Zhang, G.; Chen, H.; Zhang, G.; Han, Y.; Chang, Y.; Gong, P. Mn/beta and Mn/ZSM-5 for the low-temperature selective catalytic reduction of NO with ammonia: Effect of manganese precursors. *Chin. J. Catal.* **2018**, *39*, 118–127. [CrossRef]
31. Wang, X.; Wu, W.; Chen, Z.; Wang, R. Bauxite-supported Transition Metal Oxides: Promising Low-temperature and SO_2-tolerant Catalysts for Selective Catalytic Reduction of NOx. *Sci. Rep.* **2015**, *5*, 9766. [CrossRef]
32. Chen, H.Y.; Wei, Z.; Kollar, M.; Gao, F.; Wang, Y.; Szanyi, J.; Peden, C.H. NO oxidation on zeolite supported Cu catalysts: Formation and reactivity of surface nitrates. *Catal. Today* **2016**, *267*, 17–27. [CrossRef]
33. Liu, J.; Li, X.; Zhao, Q.; Zhang, D.; Ndokoye, P. The selective catalytic reduction of NO with propene over Cu-supported Ti–Ce mixed oxide catalysts: Promotional effect of ceria. *J. Mol. Catal. A-Chem.* **2013**, *378*, 115–123. [CrossRef]
34. Leistner, K.; Olsson, L. Deactivation of Cu/SAPO-34 during low-temperature NH_3-SCR. *Appl. Catal. B-Environ.* **2015**, *165*, 192–199. [CrossRef]
35. Wu, Z.; Jiang, B.; Liu, Y. Effect of transition metals addition on the catalyst of manganese/titania for low-temperature selective catalytic reduction of nitric oxide with ammonia. *Appl. Catal. B-Environ* **2008**, *79*, 347–355. [CrossRef]

36. Qi, G.; Yang, R.T. Low-temperature selective catalytic reduction of NO with NH_3 over iron and manganese oxides supported on titania. *Appl. Catal. B-Environ.* **2003**, *44*, 217–225. [CrossRef]
37. Worch, D.; Suprun, W.; Gläser, R. Supported transition metal-oxide catalysts for HC-SCR DeNOx with propene. *Catal. Today* **2011**, *176*, 309–313. [CrossRef]
38. Roy, S.; Baiker, A. NOx Storage−Reduction Catalysis: From Mechanism and Materials Properties to Storage−Reduction Performance. *Chem. Rev.* **2009**, *109*, 4054–4091. [CrossRef] [PubMed]
39. Santillan-Jimenez, E.; Miljković-Kocić, V.; Crocker, M.; Wilson, K. Carbon nanotube-supported metal catalysts for NOx reduction using hydrocarbon reductants. Part 1: Catalyst preparation, characterization and NOx reduction characteristics. *Appl. Catal. B-Environ.* **2011**, *102*, 1–8. [CrossRef]
40. Adamowska-Teyssier, M.; Krztoń, A.; Da Costa, P.; Djéga-Mariadassou, G. SCR NOx mechanistic study with a mixture of hydrocarbons representative of the exhaust gas from coal combustion over $Rh/Ce_{0.62}Zr_{0.38}O_2$ catalyst. *Fuel* **2015**, *150*, 21–28. [CrossRef]
41. Gu, H.; Chun, K.M.; Song, S. The effects of hydrogen on the efficiency of NOx reduction via hydrocarbon-selective catalytic reduction (HC-SCR) at low temperature using various reductants. *Int. J. Hydrogen Energy* **2015**, *40*, 9602–9610. [CrossRef]
42. Mrad, R.; Aissat, A.; Cousin, R.; Courcot, D.; Siffert, S. Catalysts for NOx selective catalytic reduction by hydrocarbons (HC-SCR). *Appl. Catal. A-Gen.* **2015**, *504*, 542–548. [CrossRef]
43. Nicolae, S.; Neaţu, F.; Florea, M. Selective catalytic oxidation reaction of p-xylene on manganese–iron mixed oxide materials. *CR Chim.* **2018**, *21*, 354–361. [CrossRef]
44. Westermann, A.; Azambre, B.; Koch, A. Effect of Ag, Pd and Co promoters on the Selective Catalytic Reduction (SCR) of NOx by ethanol over sulfated ceria-zirconia catalysts. *Catal. Today* **2012**, *191*, 65–74. [CrossRef]
45. Park, S.M.; Jang, H.G.; Kim, E.S.; Han, H.S.; Seo, G. Incorporation of zirconia onto silica for improved Pt/SiO_2 catalysts for the selective reduction of NO by H_2. *Appl. Catal. A-Gen.* **2012**, *427–428*, 155–164. [CrossRef]
46. Liu, F.; Chen, L.; Neathery, J.; Saito, K.; Liu, K. Cerium oxide promoted iron-based oxygen carrier for chemical looping combustion. *Ind. Eng. Chem. Res.* **2014**, *53*, 16341–16348. [CrossRef]
47. Komvokis, V.G.; Iliopoulou, E.F.; Vasalos, I.A.; Triantafyllidis, K.S.; Marshall, C.L. Development of optimized Cu–ZSM-5 deNOx catalytic materials both for HC-SCR applications and as FCC catalytic additives. *Appl. Catal. A* **2007**, *325*, 345–352. [CrossRef]
48. Zhang, H. *Fundamental Study on CH_4-SCR of Nox*; Zhejiang University: Hangzhou, China, 2005.
49. Yan, J.Y.; Lei, G.D.; Sachtler, W.H.M.; Kung, H.H. Deactivation of Cu/ZSM-5 catalysts for lean NOx reduction: Characterization of changes of Cu state and zeolite support. *J. Catal.* **1996**, *161*, 43–54. [CrossRef]
50. Xie, J.; Fang, D.; He, F.; Chen, J.; Fu, Z.; Chen, X. Performance and mechanism about MnO_X species included in MnO_X/TiO_2 catalysts for SCR at low temperature. *Catal. Commun.* **2012**, *28*, 77–81. [CrossRef]
51. Tamm, S.; Ingelsten, H.H.; Skoglundh, M.; Palmqvist, A.E. Mechanistic aspects of the selective catalytic reduction of NOx by dimethyl ether and methanol over γ-Al_2O_3. *J. Catal.* **2010**, *276*, 402–411. [CrossRef]
52. Tseng, H.H.; Lu, C.Y.; Chang, F.Y.; Wey, M.Y.; Cheng, H.T. Catalytic removal of NO and PAHs over AC-supported catalysts from incineration flue gas: Bench-scale and pilot-plant tests. *Chem. Eng. J.* **2011**, *169*, 135–143. [CrossRef]
53. Tang, X.; Hao, J.; Yi, H.; Li, J. Low-temperature SCR of NO with NH_3 over AC/C supported manganese-based monolithic catalysts. *Catal. Today* **2007**, *126*, 406–411. [CrossRef]
54. Marbán, G.; Antuña, R.; Fuertes, A.B. Low-temperature SCR of NOx with NH_3 over activated carbon fiber composite-supported metal oxides. *Appl. Catal. B-Environ.* **2003**, *41*, 323–338. [CrossRef]
55. Boyano, A.; Galvez, M.E.; Moliner, R.; Lazaro, M.J. Carbon based catalytic briquettes for the reduction of NO: Catalyst scale-up. *Catal. Today* **2008**, *137*, 209–214. [CrossRef]
56. Chu, Y.H.; Zhang, T.; Guo, X.J.; Liu, C.; Yin, H.Q.; Zhu, X.F.; Liu, Y.J. Low temperature selective catalytic reduction of NO by C_3H_6 over CeOx loaded on AC treated by HNO_3. *J. Rare Earth* **2015**, *33*, 371–381. [CrossRef]
57. Marbán, G.; Fuertes, A.B. Kinetics of the low-temperature selective catalytic reduction of NO with NH_3 over activated carbon fiber composite-supported iron oxides. *Catal. Lett.* **2002**, *84*, 13–19. [CrossRef]

58. Anthonysamy, S.B.I.; Afandi, S.B.; Khavarian, M.; Mohamed, A.R.B. A review of carbon-based and non-carbon-based catalyst supports for the selective catalytic reduction of nitric oxide. *Beilstein J. Nanotechnol.* **2018**, *9*, 740–761. [CrossRef] [PubMed]
59. Liu, F.; Yang, L.; Song, C. Chemical looping hydrogen production using activated carbon and carbon black as multi-function carriers. *Int. J. Hydrogen Energy* **2018**, *43*, 5501–5511. [CrossRef]
60. Liu, F.; Chen, L.; Yang, L.; Fan, Z.; Nikolic, H.; Liu, K. Application of chemical looping process for continuous high purity hydrogen production by methane thermocatalytic decomposition. *Int. J. Hydrogen Energy* **2016**, *41*, 4592–4602. [CrossRef]
61. Lin, L.; Luo, Y.; Tsai, P.; Wang, J.; Chen, X. Metal ions doped carbon quantum dots: Synthesis, physicochemical properties, and their applications. *TrAC-Trend Anal. Chem.* **2018**, *103*, 87–101. [CrossRef]
62. Kaczmarczyk, J.; Zasada, F.; Janas, J.; Indyka, P.; Piskorz, W.; Kotarba, A.; Zbigniew, S. Thermodynamic Stability, Redox Properties, and Reactivity of Mn_3O_4, Fe_3O_4, and Co_3O_4 Model Catalysts for N_2O Decomposition: Resolving the Origins of Steady Turnover. *ACS Catal.* **2016**, *6*, 1235–1246. [CrossRef]
63. Amer, A.; Reda, S.M.; Mousa, M.A.; Mohamed, M.M. Mn3O4/graphene nanocomposites: Outstanding performances as highly efficient photocatalysts and microwave absorbers. *RSC Adv.* **2017**, *7*, 826–839. [CrossRef]
64. Li, N.; Tian, Y.; Zhao, J.; Zhang, J.; Zhang, J.; Zuo, W.; Ding, Y. Efficient removal of chromium from water by Mn_3O_4@ZnO/Mn_3O_4 composite under simulated sunlight irradiation: Synergy of photocatalytic reduction and adsorption. *Appl. Catal. B-Environ.* **2017**, *7*, 126–136. [CrossRef]
65. Raj, A.M.E.; Victoria, S.G.; Jothy, V.B.; Ravidhas, C.; Wollschläger, J.; Suendorf, M.; Neumann, M.; Jayachandran, M.; Sanjeeviraja, C. XRD and XPS characterization of mixed valence Mn_3O_4 hausmannite thin films prepared by chemical spray pyrolysis technique. *Appl. Surf. Sci.* **2010**, *256*, 2920–2926.